An updated Weichselian chronostratigraphic framework of the Kongsfjorden Trough Mouth Fan and its implications for the glacial history of Svalbard

DANIEL HESJEDAL WIBERG (iD), HAFLIDI HAFLIDASON (iD) AND JAN SVERRE LABERG (iD)

BOREAS

The Arctic is a climate-sensitive area, responding rapidly to present changes, but for the past changes, the record is still incomplete. For instance, the Weichselian glacial history of the Svalbard–Barents Sea Ice Sheet (SBIS) has largely been reconstructed based on studies of the fragmentary Spitsbergen terrestrial and shelf records. However, the sediments removed from the land and shelf areas during peak glacials were deposited on trough mouth fans located along the continental slope. By studying the stratigraphy and processes of the trough mouth fans, comprising a more complete sediment archive, our new data have allowed gaps in the Weichselian glacial history of the SBIS to be refined and filled. Here we present new lithological and geochronological data from the Kongsfjorden Trough Mouth Fan, closely linked to the advance and decay of the SBIS. High-resolution TOPAS seismic profiles reveal three distinct packages of glacigenic debris flows (GDFs) within its upper stratigraphy, each interpreted to represent an advance of the SBIS to the shelf edge. A radiocarbon dated, 12.6-m-long core from the southern flank of the Kongsfjorden Trough Mouth Fan penetrates trough sediments directly linked to the youngest GDF package and terminates in the second GDF, allowing us to study the last two Kongsfjorden ice-stream advances in greater detail than was previously possible. The age model of core GS10-164-09PC, based on combining ^{14}C-, ^{18}O-stable isotope and magnetic susceptibility data, spans the last ~54 ka. An Early Weichselian glacial advance is tentatively dated to have ended at ~90 ka. A second peak glaciation is estimated at ~70 ka, followed by a deglaciation from ~54 ka. An ice rafted debris-rich unit (U7) dated between 38 and 34 ka, followed by a plumite (U6), indicates an advance of unknown extent. The Last Glacial Maximum advance is dated to before 24 ka BP, followed by a rapid deglaciation at ~15 ka. The presence of coarser-grained sorted sediments at the present seafloor is attributed to the influence of the West-Spitsbergen Current, acting on water depths of at least 846 m, and is thought to have worked in the vicinity of the coring site since ~14 ka BP.

Daniel Hesjedal Wiberg (daniel.h.wiberg@uit.no/daniel.wiberg@ngu.no), Department of Geosciences, UiT – The Arctic University of Norway, 9037 Tromsø, Norway; present address: Geological Survey of Norway (NGU), Postboks 6315, 7491 Torgarden, Trondheim, Norway; Haflidi Haflidason, Department of Earth Science, University of Bergen, 5007 Bergen, Norway and Bjerknes Centre for Climate Research, Box 7803, N-5020 Bergen, Norway; Jan Sverre Laberg, Department of Geosciences, UiT – The Arctic University of Norway, 9037 Tromsø, Norway; received 3rd February 2021, accepted 23rd December 2021.

Based on terrestrial archives it has been postulated that during the Weichselian Glacial (~118–11.6 ka), the Svalbard–Barents Sea Ice Sheet (SBIS) extended at least three times to the edge of the West-Svalbard continental margin (Fig. 1) (Mangerud *et al.* 1998; Svendsen *et al.* 2004; Hormes *et al.* 2013; Ingolfsson & Landvik 2013; Eccleshall *et al.* 2016; Alexanderson *et al.* 2018). The general understanding has been that the maximum extent was achieved around 118–108 ka (MIS 5d), 75–50 ka (MIS 4) and during the Last Glacial Maximum (LGM) 32–20.5 ka (MIS 2) (e.g. Mangerud & Svendsen 1992; Elverhøi *et al.* 1995; Jessen *et al.* 2010; Hormes *et al.* 2013). The duration of the MIS 4 glacial maximum is assumed to have been up to 20 000 years, but for the MIS 5d and LGM the time of maximum extent is assumed to have been shorter, *c.* 10 000 years. The most recent studies on terrestrial deposits from the Kongsfjorden area suggest, however, that ice advanced through Kongsfjorden towards and onto the shelf edge more frequently than previously assumed (Eccleshall *et al.* 2016; Alexanderson *et al.* 2018). Eccleshall *et al.* (2016) agree on the ice advances during MIS 5d and LGM, but instead of a third advance during MIS 4 they see evidence of an event in MIS 5b (93–83 ka). Alexanderson *et al.* (2018) suggest a far more dynamic waxing and waning ice sheet in the Kongsfjorden area, where the ice sheet may have advanced up to five times during the Weichselian period, with peaks around 110, 90, 70, 45 and 25 cal. ka BP.

During the last deglaciation (following the LGM), the ice front re-established for a short time and developed a grounding zone wedge (GZW) at a point where the width of the Kongsfjorden Trough narrows greatly (from ~30 to ~15 km) (Ottesen *et al.* 2007). The main deglaciation period is thought to have occurred between 15 and 14 cal. ka BP, possibly with a duration of only 150–300 years, mainly centred around 14.5 to 14.4 cal. ka BP (Jessen *et al.* 2010; Hormes *et al.* 2013; Lucchi *et al.* 2013, 2015). The GZW is the only evidence of a major stillstand of the ice margin before the ice retreated into the inner Kongsfjorden fjord area (Landvik *et al.* 2005; Ottesen *et al.* 2007; Hormes *et al.* 2013; Dowdeswell *et al.* 2016).
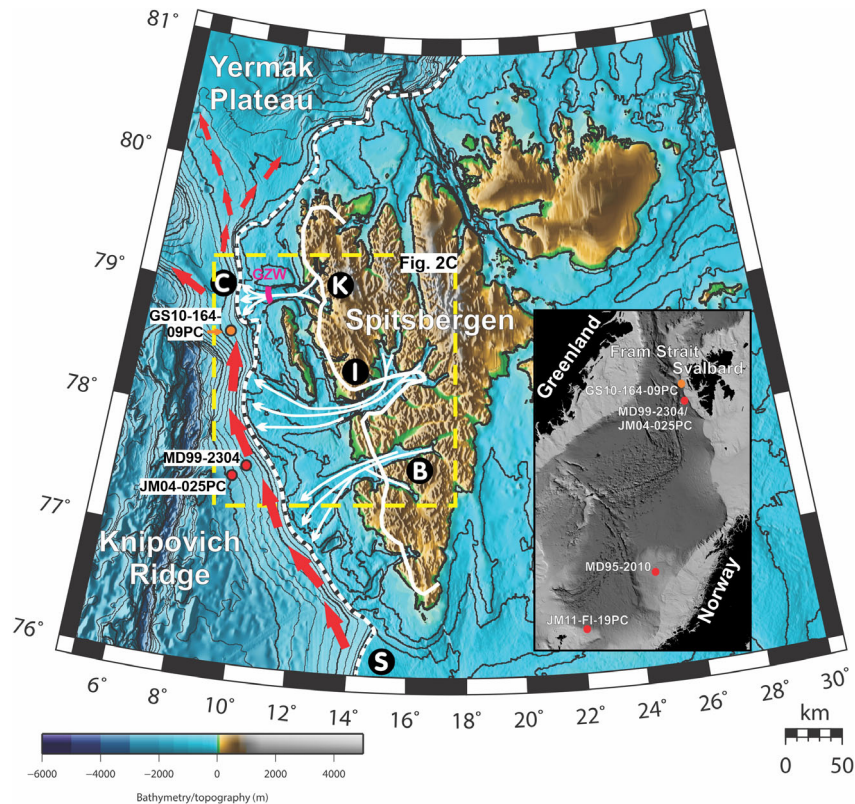
Fig. 1. Overview map of Spitsbergen and its surrounding region, with the study area outlined in yellow and the piston core GS10-164-09PC with an orange circle. The maximum extent of the Svalbard–Barents Sea Ice Sheet (Last Glacial Maximum, LGM) is marked by the white stippled line (Ottesen & Dowdeswell 2009; Hormes *et al*. 2013) and the Younger Dryas advance by solid white line (after Mangerud & Landvik 2007). The white arrows indicate the flow path of the major palaeo-ice streams along the West-Spitsbergen margin. Labelled ice streams: Ⓚ = Kongsfjorden & Krossfjorden; Ⓘ = Isfjorden; Ⓑ = Bellsund; Ⓢ = Storfjorden - Storfjorden Trough; Ⓒ = Kongsfjorden Channel System. Red arrows (after Hebbeln *et al*. 1998; Ślubowska-Woldengen *et al*. 2007) mark the West-Spitsbergen Current (WSC). The purple line indicates the location of a Grounding Zone Wedge (GZW) within the Kongsfjorden Trough (Ottesen *et al*. 2007; Dowdeswell *et al*. 2016). The map utilized the IBCAO 3.0 database (Jakobsson *et al*. 2012) and was plotted using the software GMT (Wessel & Smith 1998).

The geological record on Svalbard has been exposed to glacial erosion repeatedly and is fragmentary, and does not therefore preserve a continuous record of the Weichselian and preceding glacial periods (Mangerud *et al*. 1992; Svendsen *et al*. 1996; Forwick & Vorren 2009). Owing to repeated extensive glaciations of the Svalbard archipelago area, both on land and on the shelf, the only continuous record of the last glacial–interglacial period is located beyond the shelf edge, on the upper continental slope. The areas with the highest sedimentation rates and stratigraphical resolution are those related to the Trough Mouth Fan (TMF) sediment system, where there is a vast output of sediments from palaeo-ice streams during the glacial maxima and following deglaciations, offering the possibility of studying their processes and timing of extent to the shelf edge. While the accumulation is significantly higher during glacial than interglacial periods, some sedimentation still occurs on the TMFs during the ice-free periods (e.g. Lucchi *et al*. 2013; Carbonara *et al*. 2016). Developed on the upper part of the continental slope, TMFs represent a continuation of

the fjord and trough systems of Spitsbergen. The fjord–trough systems represent the drainage pathways of ice from the Svalbard ice cap(s) and/or the SBIS (e.g. Vorren & Laberg 1997; Landvik *et al*. 2005; Sejrup *et al*. 2005; Sarkar *et al*. 2011). The three most pronounced fan systems along the West-Spitsbergen margin are outside Kongsfjorden, Isfjorden and Bellsund (Fig. 1). It is assumed that all of these TMF systems have been active almost simultaneously during all of the peak glacial periods, owing to the narrow shelf, common source area and similarities in sedimentation in marine cores (e.g. Jessen *et al*. 2010) across the west Spitsbergen continental margin, although this remains to be proven.

The aim of this study was to use the seismo- and lithostratigraphic records retrieved from the Kongsfjorden TMF as an archive to better constrain the ice dynamics and timing of the glacial maxima of the Kongsfjorden palaeo-ice stream during the Weichselian. By refining their timing and duration, the partly conflicting results from the terrestrial archives are re-evaluated and a revised glacial chronology established.

Study area

The mountainous Svalbard archipelago (Fig. 1) is currently about 60% ice-covered and therefore is still being influenced by glacial erosion, sediment transport and deposition. The present landscape characterizing the Svalbard archipelago is the result of repeated glacial excavation, with mountainous areas separated by deeply incised valley and fjord systems. During the peak glacial periods, several ice streams overlying these valley and fjord systems were active within the SBIS. The major ice streams followed the cross-shelf troughs towards their maximal extent at the shelf edge, as is reflected in the multitude of exposed glacial morphological landforms on the continental shelf around Svalbard (Ottesen *et al.* 2005, 2007; Dowdeswell *et al.* 2008; Sarkar *et al.* 2011). Large TMFs developed outside all of the main fjord–shelf trough systems in Svalbard as a consequence of the high sediment flux during peak glacial conditions (e.g. Mangerud & Landvik 2007; Wohlfarth *et al.* 2008; Knies *et al.* 2009; Hormes *et al.* 2013; Jakobsson *et al.* 2014).

The continental margin of western Svalbard is characterized by a narrow continental shelf. It is widest outside Isfjorden (~80 km) and narrows down to ~55–60 km outside Kongsfjorden (Fig. 1). In Kongsfjorden the drainage system of the palaeo-ice stream originates in the catchment area connected to Kongsfjorden (~27–30 km) and Krossfjorden (~30 km), which fed ice into the cross-shelf trough (Howe *et al.* 2003; Ottesen *et al.* 2007; Henriksen *et al.* 2014). The Kongsfjorden cross-shelf trough has a depth between 200 and 350 m, and has an initial width of 10 km on the inner shelf, which expands to 35–40 km towards the shelf edge (Vorren *et al.* 1998; Ottesen *et al.* 2007; Batchelor & Dowdeswell 2014; Henriksen *et al.* 2014). At the shelf edge, the system terminates at the Kongsfjorden TMF, covering an area of about 2700 km^2, and extends about 55 km downslope (Vorren *et al.* 1998). On its northern flank, the Kongsfjorden Channel System is located (Fig. 1). This system consists of a series of channels, created through repeated erosion by mass movements that merge into a single main channel downslope, interpreted as having been active during peak glacial periods, when the palaeo-ice stream reached the shelf edge (Forwick *et al.* 2015).

From other TMFs along the Norwegian–Barents Sea continental margin, it is known that the sediments deposited on the TMF originated from subglacial diamictic sediments that developed into glacigenic debris flows (GDFs; e.g. Laberg & Vorren 1995; King *et al.* 1996; Dimakis *et al.* 2000). At the ice-contact zone there may also be different types of outwash materials such as coarse-grained bedload sediments and finer sediments from meltwater plumes (Lucchi *et al.* 2015). The finer sediments are thought to have emerged as a plume of sediment-laden subglacial meltwater at the glacial grounding line, further dispersed as either high-density underflows or low-density over/inflows depending on grain size (Lucchi *et al.* 2013). Meltwater plume deposits, known as plumites, are interlaminated units that generally consist of mud with occasionally coarser layers of sand (Lekens *et al.* 2005; Lucchi *et al.* 2013). A succession of GDF packages interbedded with geotechnically weaker plumites led many of the TMFs to be prone to sediment failure (Sejrup *et al.* 1996).

Within the Kongsfjorden palaeo-ice stream system, the shelf trough and fjord morphology indicate a rapid retreat, preserving mega-scale glacial lineations along the flow path (Ottesen *et al.* 2007; Sarkar *et al.* 2011). The presence of a 7.5-km broad ridge, known as a GZW, about 25 km from the shelf, indicates that there was a period of cessation in ice retreat during the last deglaciation (Ottesen *et al.* 2007; Sarkar *et al.* 2011; Dallmann *et al.* 2015).

The inflow of warm surface water from the North Atlantic to the Spitsbergen margin during the Bølling period (Ślubowska *et al.* 2005; Rasmussen *et al.* 2007; Ślubowska-Woldengen *et al.* 2007), represented by the West-Spitsbergen Current (WSC), contributed not only to a large influx of warm waters, but also to increased current velocity along the upper continental margin area. The strength of the WSC varied during the Bølling–Allerød–Younger Dryas period, but stabilized in the early part of Holocene and was found to be fairly constant in the present setting, influencing the sea floor sediments down to ~1200 m water depth (Rebesco *et al.* 2013).

Material and methods

The TOPAS profiles and the Calypso piston core used in this study were gathered in 2010 on a cruise with RV 'G.O. Sars' (Fig. 2C). The 12.66-m-long core, GS10-164-09PC, was raised from the southern part of the Kongsfjorden TMF (78°39.2953′N, 08°28.3228′E), at 846 m water depth (Figs 1, 2).

Seismic profiling

The high-resolution seismic profiles were obtained by the use of a hull-mounted TOPAS PS18 sub-bottom parametric profiler system, with a vertical resolution of 30–35 cm. The TOPAS system is attached to the electronic stabilization system of the RV 'G.O. Sars', which compensates for most of the heave, pitch and roll that affect the vessel. The maximum penetration achieved in this area is ~90 ms or ~70 m, based on the estimated P-wave seismic velocity of ~1550–1600 m s^{-1} in rather coarse glacimarine deposits.

Sediment core analyses

The split sections of core GS10-164-09PC were measured using non-destructive scanners and visually described based on colour, texture and structures before any
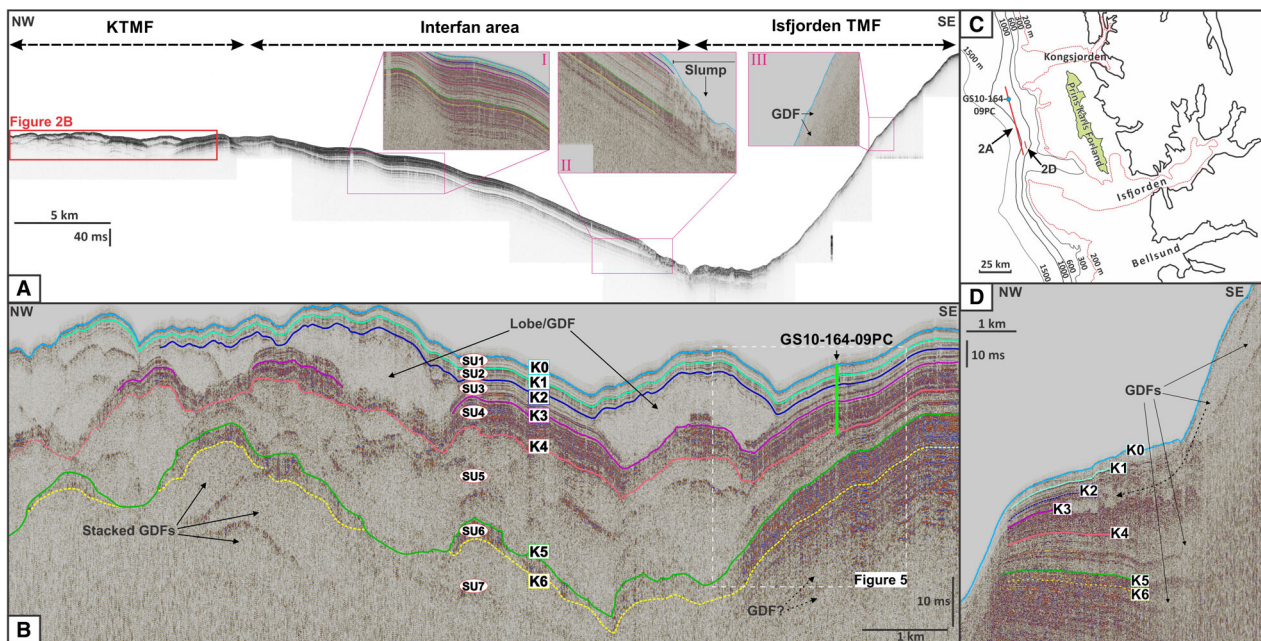
Fig. 2. A. TOPAS profile GS10-164-11 (located in Fig. 2C). In the northwestern part (red box) there are several semi-transparent lobes that are interpreted as glacigenic debris flows (GDFs). The expanded sections I–III display: (I) a section of facies SF1, undisturbed by the influence of GDFs; (II) transition into chaotic upper layers (probably caused by a slumping event); and (III) a series of GDFs where sediments of facies SF1 appear to be absent. B. Close-up view of the TOPAS profile at the core location (GS10-164-09PC; vertical green line) at Kongsfjorden Trough Mouth Fan (TMF), with the interpreted reflectors (K0–K6) and seismic units (1–7). C. Location of the study area, where seismic lines GS10-164-11 and part of GS10-164-12 is marked by red lines and the core location (blue circle) are located. D. Section of line GS10-164-12 on the northern flank of the Isfjorden TMF (located in 2C), which displays similar facies and units as seen for the Kongsfjorden TMF (see Fig. 2B).

destructive measurements or subsampling was performed. The Geotek Multi Sensor Core Logger was used to measure the gamma density and magnetic susceptibility of the sediments at a resolution of 2 mm. An ITRAX X-ray fluorescence core scanner was used to measure the element composition of the split sections at a resolution of 0.5 mm and to take X-ray images and high-resolution colour scans at a resolution of 200 μm (Fig. 3). The element ratios of Ca/Ti, Sr/Ca and K/Ti were selected to record the relative variability of these elements in the sediments, to detect changes in biological productivity, intervals with ice rafted debris (IRD) and sediment provenance. The counting results of the Ca and K element were normalized using Ti, which is considered chemically inert and therefore not susceptible to dissolution/redox changes (Croudace *et al.* 2006; Rothwell & Croudace 2015).

The undrained shear strength of the sediments was measured at 10-cm intervals with a Swedish Cone apparatus. The measurement was repeated three times and an average taken at each 10-cm interval. The shear strength is presented in kPa according to the method of Hansbo (1957).

The core was subsampled at every 10 cm using 10 mL syringes, with supplementary subsampling at critical lithological boundaries. The samples extracted were first dried for two days at 50 °C, weighed and then wet sieved. All of the samples were wet sieved using 1 mm, 125 μm

and 63 μm sieves for grain size analyses. The samples from the 1 mm and 125 μm fractions were further examined under a microscope to evaluate their potential for retrieval of microfossils for AMS ^{14}C dating. The grain size fraction larger than 1 mm reflects the occurrence of IRD in the glacimarine sediments.

Stable isotope analysis

Stable isotopes ($\delta^{18}O$ and $\delta^{13}C$, the latter not shown here) were measured where possible at ~20-cm intervals on the planktonic foraminiferal species *Neogloboquadrina pachyderma* sinistral (s) (Nps) between 200 and 600 cm depth and at ~10-cm intervals below 600-cm depth, except where the sediments are barren of Nps. The measurements were performed at the Geological Mass Spectrometry Laboratory at the University of Bergen, Norway, which has an analytical error of 0.07‰. A few duplicate samples were also measured without offsets beyond the analytical error.

Radiocarbon dating

A total of 10 samples were selected for AMS ^{14}C radiocarbon dating at the Beta Analytic Dating Laboratory, Florida (Table 1). Owing to low microfossil content, the AMS dating was performed on samples of either mixed benthic or mixed planktonic foraminifera,
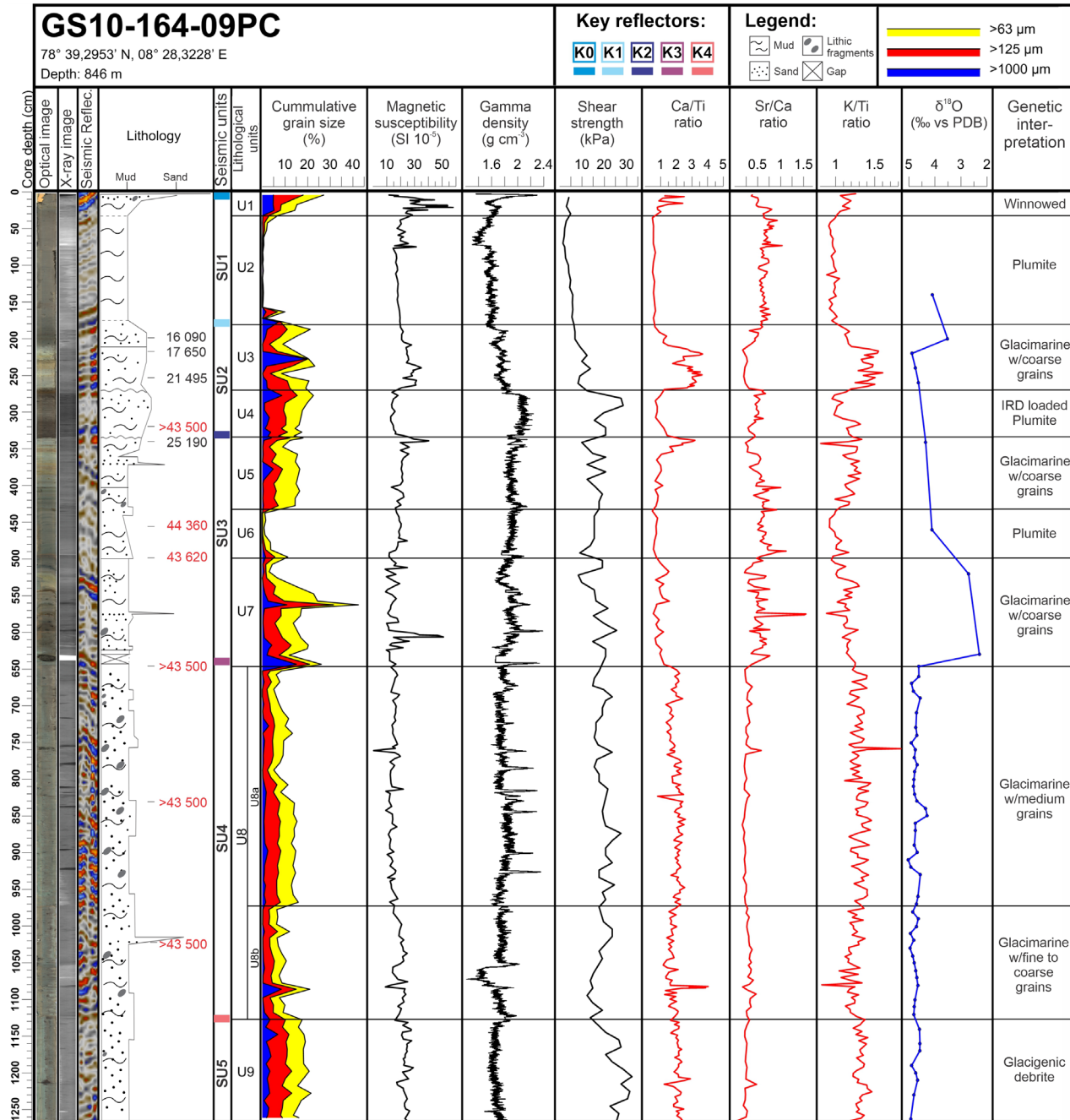
Fig. 3. Lithology of core GS10-164-09PC with optical image (core surface), X-ray image, seismic reflections image (from the TOPAS line crossing the core site), selected physical (Geotek Multi Sensor Core Logger, magnetic susceptibility, gamma density, shear strength, black curves) and chemical (X-ray fluorescence, Ca/Ti, Sr/Ca, K/Ti, red curves) properties. The blue curve represents oxygen isotope measurements, where the sample points are indicated. Cumulative grain-size distribution is given for the >63 µm (yellow), >125 µm (red) and >1000 µm (blue) fractions, the remaining fraction (summing to 100%) is <63 µm. The seismic (SU1–SU5) and lithological units (U1–U9) are also indicated, and the genetic interpretation is given. Average radiocarbon ages in the lithology column are given as cal. a BP (red text indicates ages excluded from the age model).

rather than on a single species. At three intervals, larger marine carbonate shell fragments were used for dating, consisting of six bivalve shells, shell fragments and a gastropod shell (Table 1). The AMS ¹⁴C dates were converted to calendar ages using the CALIB v. 8.1.0 program (Stuiver & Reimer 1993) and the integrated marine reservoir correction curve Marine20 (Heaton

et al. 2020). No additional local reservoir age was added to the Marine20 curve.

Results

In this section, the seismic stratigraphy, lithostratigraphy and radiocarbon measurements for the study area are

Table 1. AMS ^{14}C measurements obtained from Calypso core GS10-164-09PC. The ^{14}C ages are uncorrected for reservoir age. The measurements that gave a finite age were further converted into calendar years by the use of the Calib 8.1.0 software (Stuiver & Reimer 1993). Owing to the lack of a single dominating species, all the foraminifera samples were picked as a mix of several species to gain enough material for a reliable dating.

Laboratory ID	Depth (cm)	Core unit	[14]C age (a BP)	Calibrated age (cal. a BP)	Calendar age (2σ cal. a BP)	Material
Beta-357522	200–201.5	U3	14 010±60	16 090	16 090±265	Mixed benthic
Beta-423853	220–221.5	U3	15 260±50	17 650	17 650±280	Mixed planktonic
Beta-360143	255–256.5	U3	18 510±70	21 495	21 495±330	Mixed planktonic
Beta-360144	325–326.5	U4	>43 500	–	–	Shell fragments
Beta-360145	341–342.5	U5	21 780±90	25 190	25 190±320	Mixed planktonic
Beta-423854	460–465	U6	42 510±760	44 360	44 360±1245	Mixed planktonic
Beta-357523	500–501.5	U7	41 500±630	43 620	43 620±900	*Yoldiella lenticula*
Beta-357524	646–647.5	U8	>43 500	–	–	Mixed planktonic
Beta-357525	835–836.5	U8	>43 500	–	–	Mixed planktonic
Beta-344254	1021–1028	U8	>43 500	–	–	*Sipho gracilis*

presented. The seismic stratigraphy includes a seismic facies description (Table 2) based on Mitchum *et al.* (1977) and Lasabuda *et al.* (2018), followed by a description of the seismic units (SU1–SU7) and their bounding key reflectors (K0–K6) (Fig. 2; Table 3). These are then linked to the established lithostratigraphy for core GS10-164-09PC where possible (Fig. 3).

Seismic facies

The study area can be divided into three regional provinces, which show distinct differences in seismic characteristics: the southern Kongsfjorden Trough Mouth Fan (KTMF), the northernmost part of Isfjorden Trough Mouth Fan (ITMF), and the Interfan area (IFA) between the TMF systems, located outside Prins Karls Forland (Fig. 2). The seismic stratigraphy in this area includes four seismic facies (SF1a, SF1b, SF2 and SF3; Table 2).

SF1a: Parallel to subparallel (low amplitude). – These are very low to medium amplitude reflections, which are continuous to semi-continuous and internally laminated. They are often characterized with a conformable top and base (Table 2). SF1a is interpreted to represent deposits from hemipelagic processes. The amplitude

Table 2. Classification of the seismic facies encountered in the study area. The vertical and horizontal black bars represent 5 ms and 500 m, respectivly. The dotted black line in the figure example for SF3 indicates the border between disturbed and undisturbed sediments.
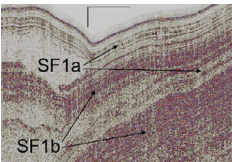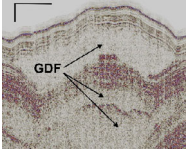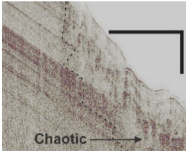
Seismic facies (SF)	Description	Interpretation	Figure example
SF1a: Parallel to subparallel (low amplitude)	Very low- to medium-amplitude reflections, continuous to semi-continuous, commonly conformable top and base	Formed from settling of sediments through the water column. Marine or glacimarine sediments with a low content of coarse material (mud rich)	
SF1b: Parallel to subparallel (high amplitude)	Medium- to very high-amplitude reflections, continuous to semi-continuous, commonly conformable top and base	Glacimarine sediments with a high content of coarse material (sand and/or ice rafted debris)	
SF2: Semi-transparent	Low-amplitude reflections, discontinuous, irregular top and base, internally structureless, single or stacked lensoid packages	Glacigenic debris flows, developed when the ice sheet is at the shelf edge	
SF3: Chaotic	Low- to high-amplitude reflections, irregular top and base, internally chaotic but some sections appear more structured; found in a small area only (Fig. 2, II)	Slumping/sliding event	

Table 3. Synthesis of the seismic and lithological units, with interpreted or inferred (in italics) depositional processes and timing.

Seismic units	Seismic facies	Key reflectors	Lithological units	Average sedimentation rate (cm ka^{-1})	Depositional mechanism	Climatic stage	Age estimate (cal. ka BP)
SU1	SF1a	K0–K1	U1, U2	180	Winnowed sediments and plumite	Meltwater pulse-1a (deglaciation) and later impacted by West-Spitsbergen Current	14–15
SU2	SF1a	K1–K2	U3, U4	17	Glacimarine and plumite	Deglaciation	15–24
SU3	SF1a, SF1b and SF2	K2–K3	U5, U6, U7	22	Glacimarine and plumite	Peak glacial	24–38
SU4	SF1b	K3–K4	U8	30	Glacimarine (high ice-rafted debris)	Deglaciation	38–54
SU5	SF1a, SF1b and SF2	K4–K5	U9	*22*	Glacigenic debris flows and inferred marine/glacimarine	Peak glacial	*54–75*
SU6	SF1b	K5–K6	Not sampled	*30*	Inferred glacimarine (high ice rafted debris)	Deglaciation	*75–90*
SU7	SF1b and SF2	K6→	Not sampled	*30*	Inferred glacigenic debris flows and glacimarine	Peak glacial	*90→*

appears to vary with the depositional process, which can be of marine or glacimarine origin (e.g. King *et al.* 1996; Nielsen & Rasmussen 2018).

SF1b: Parallel to subparallel (high amplitude). – Facies SF1b is of very similar seismic character to facies SF1a, which is continuous to semi-continuous and internally laminated facies, often with a conformable top and base. However, the reflectors exhibit medium to very high amplitudes (Table 2). SF1b is also interpreted as deposits from hemipelagic processes; however, the high amplitudes indicate the presence of coarser sediments than in SF1a. The facies is therefore interpreted as glacimarine sediments with a high content of sand and/or IRD.

SF2: Semi-transparent. – Facies SF2 is characterized by low-amplitude, discontinuous reflections which are semi-transparent to structureless. Facies SF2 appears in the seismic stratigraphy both as individual and as stacked lobes/lenses (Fig. 2B). The interval between the stacked lobes appears as a few, densely spaced reflections with a high amplitude. SF2 is interpreted as deposits from gravity-driven processes (e.g. King *et al.* 1996, 1998; Laberg & Vorren 2000), including glacigenic GDFs, based on its structureless seismic character and irregular bases.

SF3: Chaotic. – Facies SF3 is characterized by a mix of low- to high-amplitude, discontinuous reflections, i.e. a chaotic internal seismic signature with an irregular base and top (Table 2). Based on the variable amplitudes of the internal reflections, facies SF3 is interpreted to consist of slump deposits (e.g. Mitchum *et al.* 1977; Prins *et al.* 2020). Some parts of facies SF3 have a similar seismic character to the undisturbed hemipelagic facies SF1a and SF1b (Fig. 2A, II, Table 2). These areas are thought to represent blocks of more preserved hemipelagic sediment within the SF3 slump deposit.

Seismic units

Seismic unit SU7. – Seismic unit SU7 is the deepest unit defined in the study area, the base of which is not imaged and is presumed to be located deeper than the maximum signal penetration of the seismic data. SU7 is within the KTMF province, mainly comprising facies SF2, represented by semi-transparent lobes with a thickness of 5–20 ms (~4–15 m) and a width of as much as 1 km. However, this facies transforms into SF1b in the vicinity of the core site (Fig. 2B), is present throughout the IFA, then transitions back to facies SF2 within the ITMF province. The upper limit of SU7 is defined by the K6 reflector, which drapes the underlying deposits. The sedimentation within seismic unit SU7 is interpreted as being predominantly of glacimarine origin, including coarse-grained deposits; however, GDFs become dominant within both the KTMF and ITMF. SU7 is interpreted to represent the oldest occurrence of peak glacial conditions in the dataset.

Seismic unit SU6. – This unit is dominated by facies SF1b, with the top and base of the unit defined by the K5 and K6 reflectors, respectively (Fig. 2). SU6 is continuous in the IFA; however, it becomes disturbed towards the KTMF and ITMF. It has a maximum thickness of 8–10 ms (~6–8 m) in the IFA, while the preserved parts

within the KTMF are relatively thin, i.e. less than 4–5 ms (~3–4 m; Fig. 2B). SU6 is interpreted as a glacimarine unit related to the deglaciation of the oldest of the three glacial maxima identified in the study area. The disturbed seismic character of the TMFs is interpreted to be caused by later erosion by the GDFs of the overlying unit SU5.

Seismic unit SU5. – SU5 is very similar to SU7 within the KTMF, comprising mainly facies SF2, and semi-transparent lobes with a thickness of 5–15 ms (~4–12 m). The seismic facies shifts to facies SF1a close to the core site (Fig. 2B). It is present throughout the IFA, returning to facies SF2 at the ITMF province. The middle of unit SU5 in the IFA includes facies SF1b. The upper limit of SU5 is the K4 reflector. The sedimentation may be more varied in SU5 than SU6 as it comprises reflections of both facies SF1a and SF1b, possibly of both marine and/or glacimarine origin. The GDFs dominate both the KTMF and ITMF, but appear to be more widespread as they are found further SE than in unit SU7 (Fig. 2). In SU5, the erosive nature of the GDFs becomes clear as they have eroded most of unit SU6, and also slightly into SU7 within the KTMF (Fig. 2B). SU5 is interpreted to represent deposits from the (younger) peak glacial condition.

Seismic unit SU4. – This unit is also dominated by facies SF1b, with top and base defined by the K3 and K4 reflectors, respectively (Fig. 2). Unit SU4 shows clear similarities to SU6, but is not as extensively/deeply eroded (Fig. 2B). Unit SU4 is the oldest seismic unit penetrated by the core (Figs 2, 3) in its entirety. SU4 is interpreted as a glacimarine unit related to the deglaciation of the second glacial maximum in the study area. The disturbance of this unit within the TMFs is interpreted to be caused by later erosion of GDFs.

Seismic unit SU3. – SU3 shares many similarities with both units SU5 and SU7 as the KTMF province mainly includes facies SF2, which comprises both individual and stacked semi-transparent lobes. Around the core site (Fig. 2B), the SF1a facies becomes dominant and is present throughout the IFA, with the SF2 facies becoming dominant within the ITMF province (Fig. 2D). The IFA also includes facies SF1b. The upper limit of SU3 is defined around the K2 reflector (Fig. 2). GDFs become dominant within both the KTMF and the ITMF. In the IFA, the sedimentation probably includes both marine and glacimarine deposits, as in the older units SU5 and 7 (Fig. 2). SU3 is interpreted to represent the peak of the youngest glaciation recorded in the area.

Seismic unit SU2. – SU2 is dominated by facies SF1a, with internal reflectors of mainly moderate amplitudes. The internal reflectors are continuous in the IFA, and continuous to semi-continuous within both the KTMF

and the ITMF. The sediments in SU2 are interpreted to be of glacimarine origin; however, the moderate amplitude of the reflectors indicates that they may consist predominantly of finer sediments than interpreted in units SU6 and SU4. SU2 is interpreted to represent sediments from the initial deglaciation following the LGM.

Seismic unit SU1. – SU1 is characterized by facies SF1a having a very low amplitude, and is continuous throughout the study area (Fig. 2). SU1 is the youngest unit within the study area. The thickness of the unit varies with depth, and has a thickness below the seismic resolution in the shallower part of the ITMF (Fig 2A, III; 2D). SU1 originates from glacimarine and marine processes and the low amplitude indicates that the sediments are fairly homogeneous and fine grained. SU1 represents deposits from the final part of the deglaciation and the Holocene.

In summary, the Kongsfjorden TMF province is dominated by seismic facies SF2, which is found in three seismic units as semi-transparent lobes, interpreted as GDFs, resulting in an overall positive bathymetry with minor sea-floor irregularities. Facies SF1a and SF1b drape these units within the KTMF and ITMF (Fig. 2) and are the dominating facies in the IFA. Both facies are interpreted to represent glacimarine and/or marine deposits, partly eroded by the debris flows within the TMFs. SF3 is found in the IFA close to the ITMF (Fig. 2A, II) and is most likely the result of a slumping event.

Lithostratigraphy

Based on the visual, textural and structural descriptions, supported by the physical properties, X-ray fluorescence element scanning results and shear strength data, core GS10-164-09PC is divided into nine lithostratigraphic units, denoted U1–U9 (oldest).

Unit U9 (1130–1266 cm). – Unit U9 is the lowermost lithostratigraphic unit, with the lower boundary below the depth of penetration of the core. The entire unit appears visually homogeneous and consists of a grey (2.5 Y 5/1) silty clay (mud), with a consistent sand content around 20%. Grains >1000 μm make up 3–6% of the sand fraction (Fig. 3). The undrained shear strength values are the highest measured, around 25–30 kPa, and the bulk density is around ~1.6±0.2 g cm^{-3}. The magnetic susceptibility is ~23 10^{-5} SI throughout the unit, which is relatively high and stable compared with the overlying units. The Ca/Ti, K/Ti and Sr/Ca element ratios are all found to be stable throughout the unit (Fig. 3). Based on the structureless and homogeneous sandy–silty clay and high shear strength, unit U9 is interpreted to be deposited by mass movement, most likely a debris flow. This implies that the homogeneous

character is due to sediment mixing that occurred during the downslope flow.

Unit U8 (650–1130 cm). – Unit U8 is partly stratified, characterized by varying content of greyish (2.5Y 5/1) sandy–silty sediments with a sporadic content of lithic fragments of gravel and pebble size (Fig. 3). U8 also display high levels in the Ca/Ti and K/Ti ratios. Based on the sand content variability and the variation in the gamma density and Sr/Ca ratio, the unit has been subdivided into two subunits: 8a and 8b (oldest) (Fig. 3).

Subunit U8b (970–1130 cm). – Subunit U8b is 160-cm thick and consists of a partly laminated sandy–silty clay, with a sand content which varies from 8 to 10% (a short interval of 20% at ~1090 cm). The lower boundary of the unit is characterized by a drop in sand content and the shear strength values (down to ~12 kPa). In addition, the bulk density increases markedly from 1130 cm (to ~1.8 g cm^{-3}), and the Sr/Ca ratio increases (Fig. 3). A gastropod shell found at 1021–1028 cm was sent for ^{14}C dating and the results gave a non-finite radiocarbon age (Table 1).

Subunit U8a (645–970 cm). – Subunit U8a is a 325-cm-thick, weakly laminated interval consisting mainly of sandy–silty clay, with a sand content of around 15% in the lower part of the unit and 5–12% in the upper part. The proportion of grains >1000 μm is slightly higher than for subunit U8b (Fig. 3). The lower boundary is marked by a decrease in bulk density (from ~1.9 to ~1.7 g cm^{-3}) and an increase in the Ca/Ti content. All of the element ratios show a relatively low variability throughout the unit. A few large lithic fragments are present in the split core surface throughout the unit. These appear as dark zones or spots on the X-ray image (Fig. 3) and probably caused the anomalously high levels of gamma density within the unit. A batch of planktonic foraminifera was picked at 835–836.5 cm for ^{14}C age dating, but the results gave a non-finite radiocarbon age (Table 1). Subunits U8a and U8b are in general very similar in texture, structure and composition. The lamination is more pronounced and the content of larger IRD grains (lithic fragments) is somewhat higher in subunit U8a than in subunit U8b. It should be noted that there is no counting of IRD within U8 or the following units, and that the interpretation of IRD within the units is based on the presence of lithic fragments and sand content (especially the >1000-μm fraction) within the units. The Sr/Ca ratio is higher and more variable in subunit 8b than in 8a, but the ratio is constant through the whole subunit U8a. Both subunits are interpreted as comprising sediments deposited in a glacimarine environment; however, subunit U8b has a higher content of coarse IRD grains. A higher Sr/Ca content indicates a different sediment source compared with subunit U8a (Fig. 3).

Unit U7 (500–645 cm). – The lower boundary of unit U7 is defined by a significant coarsening in grain size of 5–42% (mainly ~15–20%), with an increase in the >1000 μm fraction from ~1 to ~15%. There is also a significant drop in the Ca/Ti and K/Ti ratio and a pronounced increase in the Sr/Ca ratio at this boundary. The transition into this unit is further visualized by the presence of a large lithic fragment (with a measured width and length of 7 cm and 10 cm, respectively) that filled most of the core barrel. The unit is faintly to well laminated with a marked variability in the grain size distribution (Fig. 3). The laminations of the unit consist of alternating layers of grey (2,5Y 5/1) silty clay and sandy–silty clay, with colours alternating between dark greyish brown (2,5Y 4/2) and dark grey (2,5Y 4/1). The presence of larger lithic fragments and coarser sediments within unit U7 indicates a more pronounced influx of IRD. The internal layering corresponds to variability in the Sr/Ca and K/Ti ratios. All of the element ratios measured within U7 show a significant difference in element content compared with the underlying units U8 and U9. This indicates a major shift in the sediment source area. Unit U7 is interpreted to be dominated by glacimarine deposits in a more dynamic glacial environment than the deposits of unit U8, owing to its laminated character and higher sand content.

Unit U6 (430–500 cm). – Unit U6 is characterized by a marked drop in sand content to 3–5% and has an absence of grains >1000 μm. Visually, the unit appears fairly homogeneous and is largely characterized by a dark greyish brown colour; however, several thin bands of a darker colour indicate a partly layered structure of this unit. The gamma density is constant around 1.9 g cm^{-3}, also the Ca/Ti, Sr/Ca and K/Ti/ ratios show uniform decreasing values. The shear strength initially drops to ~9 kPa, while the most of the unit lies steadily around 15 kPa (Fig. 3). Based on the homogeneous to partly laminated character and low sand content of the unit, it is interpreted as a plumite.

Unit U5 (335–430 cm). – The lower boundary of unit U5 is marked by an increase in the sand content from ~3 to ~15%, and the presence of lithic fragments (Fig. 3). The unit includes alternating layers of dark grey (2,5Y 4/1) sandy–silty clay and grey (2,5Y 5/1) silty clay. From the middle to upper parts of the unit, several well-defined rust-coloured layers appear following a gradual increase in the magnetic susceptibility. The bulk density is constant around ~1.9 g cm^{-3}, while the shear strength is fluctuating between 12 and 20 kPa. The K/Ti ratio is increasing and high through the unit while the Ca/Ti ratio starts low (0.8) and increases to a maximum of ~3.2 near the top of the unit (Fig. 3). The lithological and element characters are similar to those found in unit U7. Thus, U5 is in conformity with U7, interpreted to be of glacimarine origin. The upper part of U5 has a lighter hue compared

with the older glacimarine units, which may be due to a change in the sediment source area as indicated by the increasing Ca/Ti ratio.

Unit U4 (270–335 cm). – The lower boundary of the unit is sharp and possibly erosional. The entire unit is characterized by black to very dark grey (2,5Y 2.5/1–3/1) sandy–silty clay, where the sand content is as high as 15–20% and with a high and steady proportion of grains >1000 µm (Fig. 3). The unit appears layered, with some internal variations in colour throughout. This unit is also barren of foraminifera. The gamma density is around 2.1 g cm^{-3}, one of the highest in the core, and the magnetic susceptibility is very low through the unit (~15 SI 10^{-5}). The shear strength peaks at the top of the unit, reaching a value of ~28 kPa (Fig. 3). The Ca/Ti and K/Ti ratios is very low while the Sr/Ca ratio shows a gradual increase within the unit (Fig. 3). The base of the unit is erosive, which may indicate erosion by a gravity-driven mass movement, possibly a debris flow. Above are laminated sediments with high density and shear strength, possibly deposited from coarse-grained melt-water plumes with a high content of IRD.

Unit U3 (180–270 cm). – Unit U3 is marked by a shift in colour to a light brownish grey (2,5Y 6/2), which changes to a darker grey (2,5Y 4/1) towards the top of the unit. Intervals of rusty colour are observed around the middle part of the unit (Fig. 3). The unit is characterized by a high content of sand, fluctuating between 10 and 22%, with 3–20% of the >1000 µm fraction (Fig. 3). The magnetic susceptibility is high and the Ca/Ti and K/Ti ratios are very high, before tapering off towards the top of U3. At the lower boundary, a significant drop in both the gamma density, down to ~1.7 g cm^{-3}, and the shear strength, down to ~5 kPa is recorded. The Sr/Ca ratio has similar values to those found in units U9 and U8a, i.e. the lowest measured in the core (Fig. 3). The partly stratified sandy–silty clay with a high variability of IRD and high Ca/Ti ratio point to glacimarine sediments, deposited within a period of high biogenic productivity.

Unit U2 (30–180 cm). – Unit U2 consists mainly of a dark grey (2,5Y 4/1), homogeneous silty clay that is barren of foraminifera and contains less than ~2% sand (~5–10% at the base). The unit is mainly homogeneous, but occasional weak layering occurs throughout. The measured physical properties display a uniform, slightly decreasing trend towards the top of the unit, with a gamma density of around 1.6 g cm^{-3} and a shear strength of only around 2–5 kPa (Fig. 3). The magnetic susceptibility (~18 SI 10^{-5}), Ca/Ti and K/Ti ratios are low and stable throughout U2 while the Sr/Ca ratio is high and stable. Owing to the overall sedimentological character, similar to that of U6, with homogeneous to weakly laminated character and low sand content, unit U2 is interpreted to be a plumite (Fig. 3).

Unit U1 (0–30 cm). – Unit U1 makes up the uppermost 30 cm of the core and consists of a dark grey (2,5Y 4/1) sandy–silty clay. The grain size coarsens significantly upwards from 5 to 28% (~5% of the >1000 µm fraction), where the topmost 3 cm of the unit is sorted sand (Fig. 3). The magnetic susceptibility (25–30 SI 10^{-5}) is high and the gamma density is gradually increasing to peak at 2.4 g cm^{-3} at the core top. The coarsening towards sorted sandy sediments at the seabed is interpreted to be due to winnowing from the northward-flowing WSC.

In summary, the majority of the sedimentological units within core GS10-164-09PC are interpreted to be of glacimarine origin (Fig. 3). Most of the lower half (640–1130 cm, U8) appears to consist of glacimarine sediments with a high IRD content (sand and lithic fragments), while the unit U9 (1130–1266 cm) is interpreted to be part of a glacigenic debris flow. Similar deposits are also found in units U7, U5 and U3, although with slightly different physical properties. Lithological units U6 and U2 are both fine grained and appear to have similar physical properties trends. Both units appear to be without IRD and are interpreted as plumites. Unit U4, homogeneous with some internal layering, high density and shear strength, and non-finite dating results, is interpreted to be an IRD-loaded plumite, overlying a small mass movement deposit. The top unit (U1) coarsens upwards into a sorted sand, probably caused by winnowing by along-slope currents.

AMS ^{14}C measurements

Within the uppermost 2 m of core GS10-164-09PC, the samples were either barren of microfossils or the specimens were too few to be dated. Hence, no reliable radiometric dating could be established for this interval. Below the barren interval, four of the 10 samples for AMS ^{14}C-dating returned a finite radiocarbon age (Table 1). The six remaining samples returned either non-finite radiocarbon ages (>43 500) or ages at or near the outer limit of the radiocarbon method, and thus need to be treated with caution. The four finite ^{14}C dates, from between 200 and 350 cm depth, are used to establish the chronological framework for the upper ~4 m of the core (Fig. 3). The chronology of the interval covering the uppermost 2 m has been further refined by correlation to the dated magnetic susceptibility reference curve of Jessen *et al.* (2010). In this study, we have attempted to carry this approach further by correlating the magnetic susceptibility curve from our core with other long and dated cores (Fig. S1), with the aim of establishing a reliable age model for the deepest part of the core. Correlation to the δ^{18}O curve and Heinrich events identified in core JM04-025PC (Jessen & Rasmussen 2015, 2019) have also played a key role in further constraining and ratifying the chronology for the oldest part of the core stratigraphy (Fig. S2, Data S1).

The chronostratigraphy of the upper Kongsfjorden TMF

By correlating the age model of GS10-164-09PC established in Data S1 to the seismic stratigraphy (Fig. 4), we are able to gain further insight into the chronostratigraphy of the upper Kongsfjorden TMF. As GS10-164-09PC terminates within one of the GDF lobes related to SU5 (Fig. 2B), a direct correlation can only be carried out for seismic units SU1–SU4 and key reflectors K0–K4. This correlation is presented in Table 3. Average sedimentation rates were calculated for SU1–SU4 based on the estimated ages of K0–K4.

While SU5–SU7 lack ground truthing, seismic analysis combined with extrapolated sedimentation rates provides a tentative estimate of their ages as they share seismic facies characteristics with other cored units (SU5 is comparable with SU3, and SU6 with SU4). Based on the extrapolation of the sedimentation rates calculated for SU3 and SU4, to SU5 and SU6, a depositional period for this interval is ~20 and ~15 ka, respectively. Based on this estimate, the age of K5 is ~75 ka and that of K6 is ~90 ka (Fig. 5, Table 3). As the base of SU7 is not identified, is it not possible to estimate the age of this unit.

The Weichselian glacial history of the Kongsfjorden Trough Mouth Fan

While there is a consensus on the occurrence of several glacial advances towards the shelf edge during the Weichselian, there is still some uncertainty in both their number and timing owing to the incompleteness of the terrestrial record (e.g. Mangerud *et al.* 1998; Eccleshall *et al.* 2016; Alexanderson *et al.* 2018). With
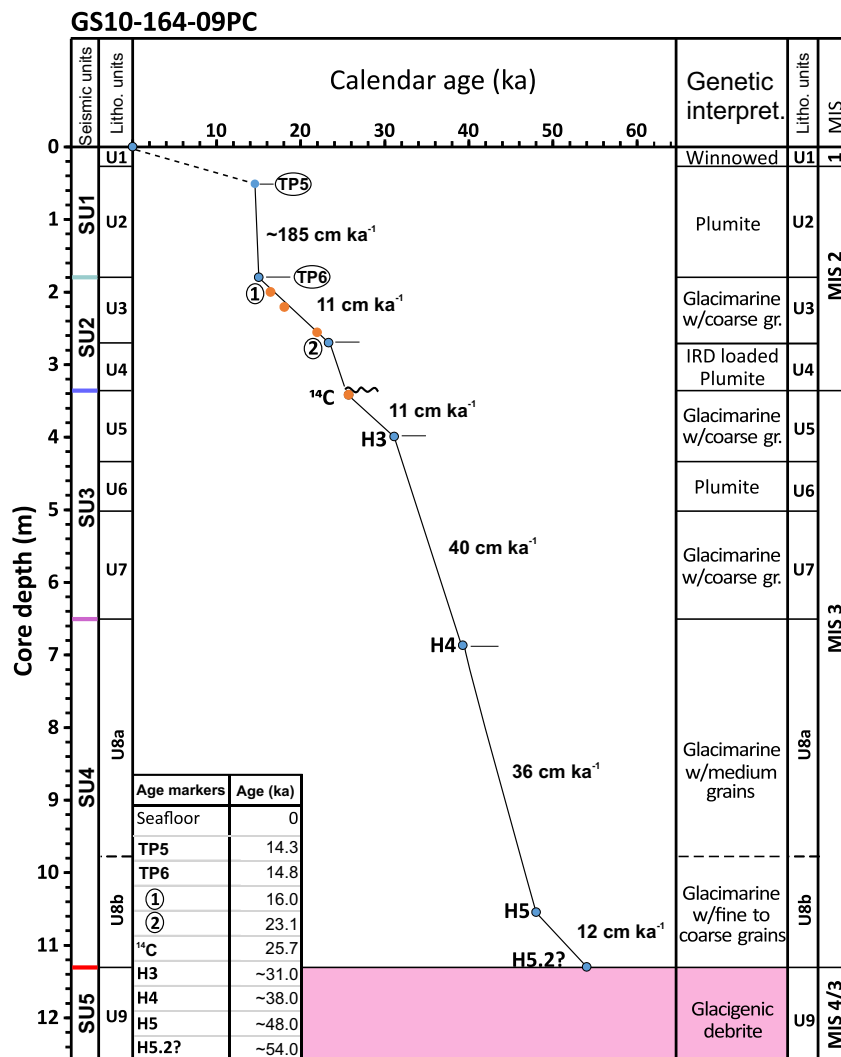

Fig. 4. The age model of core GS10-164-09PC based on radiocarbon dating, stable oxygen isotope points and MS correlation. The base is interpreted to be ~54 ka through correlation to the age models by Dokken & Jansen (1999), Hoff *et al.* (2016) and Waelbroeck *et al.* (2019). U9 is interpreted as a GDF deposit, and the interval covered by it is therefore considered instantaneous in the age model (marked in purple).
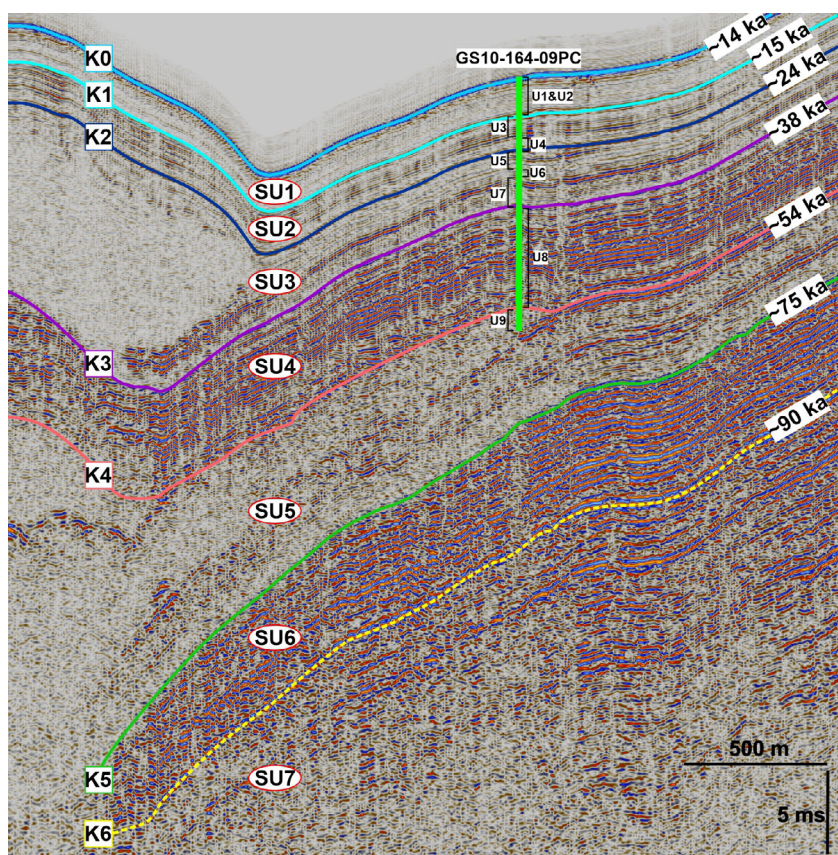
Fig. 5. Core location (green) as marked in Fig. 2B, with the estimated age of the key reflectors and units on the upper Kongsfjorden TMF. The estimated ages of reflectors K0–K4 are based on the age model from GS10-164-09PC, while the K5 and K6 estimates are based on extrapolation of sedimentation rates from seismic units SU3 and SU4 to SU5 and SU6 respectively.

the new stratigraphical framework for the Kongsfjorden TMF, we aim to better constrain the number and timing of ice advances to the shelf edge, i.e. give a better timing of the peak glacial periods in this part of the Arctic.

Based on the age model for core GS10-164-09PC, K6, the oldest reliable reflector that can be traced both within and beyond the KTMF, has an age of ~90 ka. In the lower right part of TOPAS profile GS10-164-11 (Fig. 2B) there are reflections of facies SF2 below K6 that may indicate GDFs from older ice advances to the shelf edge (MIS 5d or 6?). However, limited seismic penetration does not allow us to validate this (Figs 2, 5). The periods to be discussed here will therefore be the Weichselian and the Holocene.

The Early Weichselian (MIS 5)

The K6 reflector gives a maximum age of the GDFs in SU7 and marks the base of the oldest glacial maximum for the Kongsfjorden TMF in our data. The deposits immediately overlying SU6 are interpreted to mark the retreat and/or break-up of the Kongsfjorden palaeo-ice stream at ~90 ka.

The termination of GDFs at ~90 ka also seems to fit well with the model of Eccleshall *et al.* (2016), who suggested that the Isfjorden palaeo-ice stream reached the shelf at ~90 ka (MIS 5b). However, the original model by Mangerud *et al.* (1998), also adopted by Ingolfsson & Landvik (2013), suggests that a shelf edge glaciation outside Isfjorden terminated around 108 ka (MIS 5d), and that only minor ice advance limited to the head of the Isfjorden occurred during MIS 5b (Fig. 6). The regional ice-sheet reconstructions, developed for the Barents Sea and the Kara Sea areas by Svendsen *et al.* (2004), also supported by Larsen *et al.* (2006), suggest that an extensive ice sheet covered Svalbard during the 100–90 ka period. The evidence of an active ice stream at the shelf edge around ~90 ka is therefore not considered to be isolated to the Kongsfjorden area, but has probably been a more extensive glaciation event affecting western Svalbard.

At around 85 ka, the Kapp Ekholm site in Isfjorden is interpreted to be ice free according to Eccleshall *et al.* (2016), but there is evidence of some minor ice in the area according to Mangerud *et al.* (1998). Eccleshall *et al.* (2016) link this amelioration period with the Kapp Ekholm interstadial unit F and stage MIS 5a (~85–
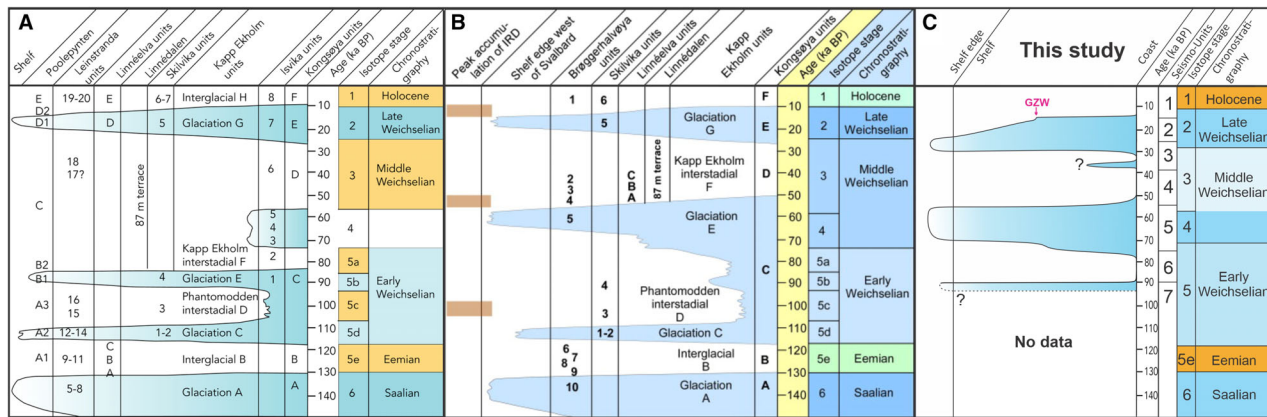
Fig. 6. Glaciation curves for the Svalbard–Barents Sea Ice Sheet through the Weichselian from Eccleshall *et al.* (2016) (A), from Ingolfsson & Landvik (2013) based on Mangerud *et al.* (1998) (B) and based on the age model of GS10-164-09PC and the seismic stratigraphy of this study (C). The question mark for the advance at 36±2 ka indicates the uncertainty of its extent, while the question mark at 90 ka indicates the tentative age estimate.

75 ka), whereas Mangerud *et al.* (1998) interpret the same interstadial unit F to be younger and of middle-late MIS 3 age (~50–28 ka; Fig. 6). In a recent study by Alexanderson *et al.* (2018), interstadial deposits were identified and described from the outer Kongsfjorden (at the Kongfjordhallét), indicating that a pronounced amelioration period also occured in the the Kongsfjorden area at ~85 ka. The glacimarine type of deposits that characterize the seismic unit SU6 on the slope off Kongsfjorden and further south, outside the Prins Karls Forland, also supports an ice-free shelf area after the ~90 ka shelf-edge glaciation period (Figs 2, 5, 6).

Following the amelioration period in the Svalbard area, centred around MIS 5a, the ice advanced again and reached the shelf edge of Kongsfjorden at ~75 ka. The evidence of long-lasting GDF activity in the KTMF records indicates that the shelf area was glaciated until ~54 ka (MIS 4 and into MIS 3). The MIS 4 glacial period (~75–57 ka) is also considered to be the most extensive Weichselian glaciation in the Barents and the Kara Seas prior to the LGM (Svendsen *et al.* 2004). Alexanderson *et al.* (2018) found evidence of a high sea-level stand at sites from outer Kongsfjorden, dated to 60±4 ka, supporting a glacial depression of the area prior to that time. Tracing the reflectors K5 and K4 from KTMF and south to the ITMF, it is also clear that the Isfjorden palaeo-ice stream extended to the shelf edge, producing GDFs within the same time frame as found in the Kongsfjorden system (Fig. 2). This is also the conclusion reached by Mangerud *et al.* (1998), whereas the ice–distance model of Eccleshall *et al.* (2016) shows that the MIS 4 ice advance only just reached the Kapp Ekholm site (Fig. 6). Our findings of active production of GDFs in SU5, on both on KTMF and the ITMF, supports the West Spitsbergen area being glaciated over a long time period around MIS 4, as well as the overall interpretation of extensive MIS 4 ice sheet cover in the polar region in this period, previously estimated to be at its maximum

extent between 70 and 60 ka (e.g. Mangerud *et al.* 1998; Svendsen *et al.* 2004; Alexanderson *et al.* 2018).

The Mid-Weichselian (MIS 3)

After the termination of the MIS 4 glacial period at ~54 ka, the Kongsfjorden palaeo-ice stream retreated from the shelf edge. The period that followed was dominated by climatic amelioration and deposition of a rather homogenous unit of glacimarine sediments (SU4/U8) until ~38 ka (Figs 2, 3, 5). Even though the MIS 3 interstadial is characterized by open ocean conditions along the West-Spitsbergen margin, this ameliorating period is generally thought to have occurred between ~45 and 30 ka (e.g. Andersen *et al.* 1996; Larsen *et al.* 2006; Mangerud *et al.* 2008; Hughes *et al.* 2016).

In the marine record, the sediment character changes from predominantly facies SF1b to predominantly facies SF1a above the regional K3 reflector. This change is thought to have occurred at ~38 ka (Figs 2, 3, 5). In core GS10-164-09PC the lower part of lithological unit U7 is found to be the coarsest and the most IRD-influenced part of the core stratigraphy, modelled to ~38 to ~34 ka (Figs 3, 4, 5). This period of extensive IRD influx coincides with the indication of a growing ice dome somewhere in the Barents Sea and/or the Svalbard archipelago (Pope *et al.* 2016; Alexanderson *et al.* 2018). Following this period of high IRD influx within the lower part of unit U7, the sedimentation shifted gradually to more fine-grained deposition (upper unit U7) and then into fine-grained plumite deposition (unit U6) from ~34 to ~32 ka in the age model (Figs 3, 4, 5).

The Last Glacial Maximum (MIS 2)

The uppermost part of seismic unit SU3, correlated with lithological unit U5, is interpreted to represent the

initiation of the LGM and a return of the Kongsfjorden palaeo-ice stream to the shelf edge (Figs 2, 3, 5). The onset of the LGM is marked with an increase of glacimarine sediments from ~32 ka, based on a pronounced increase in the coarseness of the sediment and IRD content (unit U5). Unit U5 also corresponds to the accumulation of the GDFs identified in SU3 (Figs 2, 5). As the key reflector K2 drapes the youngest GDF unit within the KTMF system, the Kongsfjorden palaeo-ice stream must have been active at the shelf edge prior to ~24 ka (Figs 2, 3, 4, 5).

Several other studies have identified a lithological unit of similar age and composition as unit U4 of GS10-164-09PC (e.g. Laberg & Vorren 1995; Jessen *et al.* 2010; Lucchi *et al.* 2013; Rasmussen & Thomsen 2013; Chauhan *et al.* 2014), where it is generally described as a massive and unsorted, very dark grey diamicton, similar to the base of U4 in this study. The unit U4 is interpreted here as an IRD-loaded plumite overlying a GDF-type deposit within the Kongsfjorden TMF. While there are some minor deviations in the age estimates of these deposits, the consensus suggests that the maximum ice extent was achieved around 26–24 ka (where recent studies lean towards the younger part of the estimate). This glacial maximum is thought to have lasted for ~10 000 years. The estimated timing of maximum ice extent at Kongsfjorden is earlier than that of the shelf area further south, along the western Barents Sea margin (Hughes *et al.* 2016), but is considered a reasonable estimate given that the shelf is narrower off Kongsfjorden. The ice would therefore have had less distance to travel to the shelf edge here.

The deglaciation and the Holocene

The earliest signs of the last deglaciation in this area are dated to around 20 ka, where the influx of IRD increases in sediment cores from the West-Spitsbergen margin (Hormes *et al.* 2013). In GS10-164-09PC there is a glacimarine unit containing IRD from about 23 ka (U3); however, the first clear sign of a break-up of the SBIS is the initial deposition of meltwater plumites defined at the base of U2, dated to ~15 ka (Figs 3, 4, 5). A unit of similar age and composition has been identified in several cores from the Svalbard margin (e.g. Rasmussen *et al.* 2007; Jessen *et al.* 2010; Lucchi *et al.* 2013; Chauhan *et al.* 2014). The plumite interval (U2) in GS10-164-09PC is among the more massive with a thickness of 150 cm; however, thicker units have been identified further south along the margin (Lucchi *et al.* 2013). The glacial retreat and following meltwater plume appear to have occurred almost simultaneously over large areas covered by the SBIS from 15 to 14.2 ka, and is connected to an event known as meltwater pulse 1a (MWP-1a; e.g. Rasmussen *et al.* 2007; Lucchi *et al.* 2013).

Two scenarios for the origin of this plume may apply: (i) the retreat marks the end of the presence of SBIS on the outer shelf, with the suspended sediments deposited as it retreated from the shelf edge and towards the GZW ~35 km from Spitsbergen, identified by Ottesen *et al.* (2007); and (ii) the initial retreat occurred earlier than 15 ka and at a slower rate, where the meltwater plume was related to a final retreat from the GZW and towards the mainland of Spitsbergen. Both scenarios are currently plausible as the origin and timing of the GZW in Kongsfjorden are still unknown (Dowdeswell *et al.* 2016); however, a similar development to the second scenario is suggested by Hormes *et al.* (2013). This is further substantiated by the core NP90-11 located a short distance behind the GZW, where a laminated unit similar to U2 is deposited on top of a diamicton, and is dated to 14 510±430 a BP (recalibrated with Marine20; Landvik *et al.* 2005).

The sorted, sandy sediment of unit U1 (Fig. 3) indicates that winnowing by a bottom current has eroded the finer material. According to Rebesco *et al.* (2013), there is presently a strong ocean current, the WSC, down to about 1200 m water depth along the West-Spitsbergen slope. The sediment core was retrieved from a depth of 846 m, which is well within the 1200 m depth range of the current. Observations by Ślubowska-Woldengen *et al.* (2007) indicate that an inflow of Atlantic Water occurred during the Bølling–Allerød interstadial, starting around 15 ka, and with an increased effect from 14.3 ka. By these estimates, it becomes apparent that the WSC started to rework the sediments at the seabed shortly after the start of the break-up of the LGM ice sheet. The winnowing effect by the WSC has been confirmed to be absent in deeper cores in the area (e.g. Jessen *et al.* 2010; Sztybor & Rasmussen 2017), where dating indicates sedimentation throughout the Holocene.

According to the age model (Fig. 4) and the winnowed surface of GS10-164-09PC, it is clear that the sediment supply to the Kongsfjorden TMF almost completely stagnated, and the WSC dominated among the active processes. The later advance of the ice sheet during the Younger Dryas is not identified in the record, probably owing to the impact of the WSC at the core site and the distance to the source area. The Younger Dryas advance (Fig. 1) appears to have halted within the fjords, close to the mouth where Kongsfjorden and Krossfjorden meet (Skirbekk *et al.* 2010), and while Mangerud & Landvik (2007) suggested that some glaciers during the LIA may have advanced further than during the Younger Dryas in a few areas of Spitsbergen, this does not appear to be the case for Kongsfjorden.

Conclusions

- The upper stratigraphy of Kongsfjorden TMF consists of packages of gravity-driven GDFs, a slump deposit and hemipelagic processes. The GDFs appear

as single or stacked deposits, marking a glacial maxima at the shelf edge.

- In this study, we have identified three major advances of the SBIS to the shelf edge, and a minor ice advance beyond the coast. The earliest advance is tentatively estimated to ~90 ka, the second is dated to ~70–60 ka and the third is thought to represent the peak of the LGM when the ice sheet reached the shelf edge prior to 24 ka.

- An influx of IRD-rich sediments followed by a plumite, dated to between 38 and 34 ka, suggests a short-lived advance of the SBIS onto the shelf; however its extent is unknown.

- The onset of the LGM can be seen from ~32 ka, and the following break-up and retreat are considered to have progressed at a steady rate, until ~15 ka BP, when rapid deglaciation towards the coast occurred.

- The WSC started to influence the study area from ~14 ka BP, and restricted further sedimentation at the core site.

- At this point, the magnetic susceptibility-method needs more refining, including dating points from other methods; however, the application of the magnetic susceptibility parameter was found to be useful for correlation and constraining the chronological model of the core. It also seems to have the potential to become a useful and inexpensive method to establish a regional chronological framework of marine cores in the low-high Arctic.

Author contributions. – This project was initiated and developed by HH. He was also the cruise leader when the sediment core and the seismic profiles were acquired. DHW conducted all laboratory analyses of the sediment core, did the seismic analysis and wrote the first draft of the manuscript. HH supervised the analysis. HH and JSL participated in the data interpretation and in formulations and modifications on the manuscript. The authors declare no conflict of interest.

Data availability statement. – The data that support the findings of this study are available from the corresponding author upon request.

References

Alexanderson, H., Henriksen, M., Ryen, H., Landvik, J. & Peterson, G. 2018: 200 ka of glacial events in NW Svalbard: an emergence cycle facies model and regional correlations. *The Journal of Arctic Geosciences 4*, 1–25.

Andersen, E., Dokken, T., Elverhoei, A., Solheim, A., Fossen, I. & Andersen, E. 1996: Late Quaternary sedimentation and glacial history of the western Svalbard continental margin. *Marine Geology 133*, 123–156.

Batchelor, C. L. & Dowdeswell, J. A. 2014: The physiography of High Arctic cross-shelf troughs. *Quaternary Science Reviews 92*, 68–96.

Carbonara, K., Mezgec, K., Varagona, G., Musco, M. E., Lucchi, R. G., Villa, G., Morigi, C., Melis, R. & Caffau, M. 2016: Palaeoclimatic changes in Kveithola, Svalbard, during the Late Pleistocene deglaciation and Holocene: Evidences from microfossil and sedimentary records. *Palaeogeography, Palaeoclimatology, Palaeoecology 463*, 136–149.

Chauhan, T., Rasmussen, T. L., Noormets, R., Jakobsson, M. & Hogan, K. A. 2014: Glacial history and paleoceanography of the southern Yermak Plateau since 132 ka BP. *Quaternary Science Reviews 92*, 155–169.

Croudace, I. W., Rindby, A., Rothwell, R. G. & Rothwell, R. G. 2006: ITRAX; description and evaluation of a new multi-function X-ray core scanner. *Geological Society Special Publications 267*, 51–63.

Dallmann, W. K., Forwick, M., Laberg, J. S. & Vorren, T. 2015: Physical geography. *In* Dallmann, W. K. (ed.): *Geoscience atlas of Svalbard*, 19–30, Norsk polarinstitutt, Tromsø.

Dimakis, P., Elverhøi, A., Høeg, K., Solheim, A., Harbitz, C., Laberg, J. S., Vorren, T. O. & Marr, J. 2000: Submarine slope stability on high-latitude glaciated Svalbard-Barents Sea margin. *Marine Geology 162*, 303–316.

Dokken, T. & Jansen, E. 1999: Age model of sediment core MD95-2010. In supplement to: Dokken, T. & Jansen, E. 1999: Rapid changes in the mechanism of ocean convection during the last glacial period. *Nature 401*, 458–461.

Dowdeswell, J. A., Ottesen, D., Evans, J., Ó Cofaigh, C. & Anderson, J. B. 2008: Submarine glacial landforms and rates of ice-stream collapse. *Geology 36*, 819–822.

Dowdeswell, J. A., Ottesen, D. & Forwick, M. 2016: Grounding-zone wedges on the western Svalbard shelf. *Geological Society, London, Memoirs 46*, 233–234.

Eccleshall, S. V., Hormes, A., Hovland, A. & Preusser, F. 2016: Constraining the chronology of Pleistocene glaciations on Svalbard: Kapp Ekholm re-visited. *Boreas 45*, 790–803.

Elverhøi, A., Svendsen, J. I., Solheim, A., Andersen, E. S., Milliman, J., Mangerud, J. & Hooke, R. L. 1995: Late Quaternary Sediment Yield from the High Arctic Svalbard Area. *The Journal of Geology 103*, 1–17.

Forwick, M. & Vorren, T. O. 2009: Late Weichselian and Holocene sedimentary environments and ice rafting in Isfjorden, Spitsbergen. *Palaeogeography, Palaeoclimatology, Palaeoecology 280*, 258–274.

Forwick, M., Laberg, J., Hass, H. & Osti, G. 2015: The Kongsfjorden Channel System offshore NW Svalbard: downslope sedimentary processes in a contour-current-dominated setting. *The Journal of Arctic Geosciences 1*, 1–16.

Hansbo, S. 1957: A new approach to the determination of the shear strength of clay by the fall-cone test. *Proceedings of the Royal Swedish Geotechnical Institute 14*, 7–47.

Heaton, T. J., Köhler, P., Butzin, M., Bard, E., Reimer, R. W., Austin, W. E. N., Bronk Ramsey, C., Grootes, P. M., Hughen, K. A., Kromer, B., Reimer, P. J., Adkins, J., Burke, A., Cook, M. S., Olsen, J. & Skinner, L. C. 2020: Marine20—The Marine Radiocarbon Age Calibration Curve (0–55,000 Cal BP). *Radiocarbon 62*, 779–820.

Hebbeln, D., Henrich, R. & Baumann, K.-H. 1998: Paleoceanography of the Last Interglacial/Glacial Cycle in the Polar North Atlantic. *Quaternary Science Reviews 17*, 125–153.

Henriksen, M., Alexanderson, H., Landvik, J. Y., Linge, H. & Peterson, G. 2014: Dynamics and retreat of the Late Weichselian Kongsfjorden ice stream, NW Svalbard. *Quaternary Science Reviews 92*, 235–245.

Hoff, U., Rasmussen, T. L., Stein, R., Ezat, M. M. & Fahl, K. 2016: Sea ice and millennial-scale climate variability in the Nordic seas 90 kyr ago to present. *Nature Communications 7*, 12247, https://doi.org/10.1038/ncomms12247.

Hormes, A., Gjermundsen, E. F. & Rasmussen, T. L. 2013: From mountain top to the deep sea - Deglaciation in 4D of the northwestern Barents Sea ice sheet. *Quaternary Science Reviews 75*, 78–99.

Howe, J. A., Moreton, S. G., Morri, C. & Morris, P. 2003: Multibeam bathymetry and the depositional environments of Kongsfjorden and Krossfjorden, western Spitsbergen, Svalbard. *Polar Research 22*, 301–316.

Hughes, A. L. C., Gyllencreutz, R., Lohne, Ø. S., Mangerud, J. & Svendsen, J. I. 2016: The last Eurasian ice sheets – a chronological database and time-slice reconstruction, DATED-1. *Boreas 45*, 1–45.

Ingolfsson, O. & Landvik, J. Y. 2013: The Svalbard-Barents Sea ice-sheet - Historical, current and future perspectives. *Quaternary Science Reviews 64*, 33–60.

Jakobsson, M., Andreassen, K., Bjarnadóttir, L. R., Dove, D., Dowdeswell, J. A., England, J. H., Funder, S. Hogan, K., Ingólfsson, Ó., Jennings, A., Krog Larsen, N., Kirchner, N., Landvik, J. Y., Mayer, L., Mikkelsen, N., Möller, P., Niessen, F., Nilsson, J., O'Regan, M., Polyak, L., Nørgaard-Pedersen, N. & Stein, R. 2014: Arctic Ocean glacial history. *Quaternary Science Reviews 92*, 40–67.

Jakobsson, M., Mayer, L., Coakley, B., Dowdeswell, J. A., Forbes, S., Fridman, B., Hodnesdal, H., Noormets, R., Pedersen, R., Rebesco, M., Schenke, H. W., Zarayskaya, Y., Accettella, D., Armstrong, A., Anderson, R. M., Bienhoff, P., Camerlenghi, A., Church, I., Edwards, M., Gardner, J. V., Hall, J. K., Hell, B., Hestvik, O., Kristoffersen, Y., Marcussen, C., Mohammad, R., Mosher, D., Nghiem, S. V., Pedrosa, M. T., Travaglini, P. G. & Weatherall, P. 2012: The International Bathymetric Chart of the Arctic Ocean (IBCAO) Version 3.0. *Geophysical Research Letters 39*, L12609, https://doi.org/10.1029/2012GL052219.

Jessen, S. P. & Rasmussen, T. L. 2015: Sortable silt cycles in Svalbard slope sediments 74–0 ka. *Journal of Quaternary Science 30*, 743–753.

Jessen, S. P. & Rasmussen, T. L. 2019: Ice-rafting patterns on the western Svalbard slope 74–0 ka: interplay between ice-sheet activity, climate and ocean circulation. *Boreas 48*, 236–256.

Jessen, S. P., Rasmussen, T. L., Nielsen, T. & Solheim, A. 2010: A new Late Weichselian and Holocene marine chronology for the western Svalbard slope 30,000–0 cal years BP. *Quaternary Science Reviews 29*, 1301–1312.

King, E. L., Haflidason, H., Sejrup, H. P. & Løvlie, R. 1998: Glacigenic debris flows on the North Sea Trough Mouth Fan during ice stream maxima. *Marine Geology 152*, 217–246.

King, E. L., Sejrup, H. P., Haflidason, H., Elverhøi, A. & Aarseth, I. 1996: Quaternary seismic stratigraphy of the North Sea Fan: glacially-fed gravity flow aprons, hemipelagic sediments, and large submarine slides. *Marine Geology 130*, 293–315.

Knies, J., Matthiessen, J., Vogt, C., Laberg, J. S., Hjelstuen, B. O., Smelror, M., Larsen, E., Andreassen, K., Eidvin, T. & Vorren, T. O. 2009: The Plio-Pleistocene glaciation of the Barents Sea-Svalbard region: a new model based on revised chronostratigraphy. *Quaternary Science Reviews 28*, 812–829.

Laberg, J. S. & Vorren, T. O. 1995: Late Weichselian submarine debris flow deposits on the Bear Island Trough mouth fan. *Marine Geology 127*, 45–72.

Laberg, J. S. & Vorren, T. O. 2000: Flow behaviour of the submarine glacigenic debris flows on the Bear Island Trough Mouth Fan, western Barents Sea. *Sedimentology 47*, 1105–1117.

Landvik, J. Y., Ingólfsson, Ó., Mienert, J., Lehman, S. J., Solheim, A., Elverhøi, A. & Ottesen, D. 2005: Rethinking Late Weichselian ice-sheet dynamics in coastal NW Svalbard. *Boreas 34*, 7–24.

Larsen, E., Kjaer, K., Funder, S. & Groesfjeld, K. Houmark-Nielsen, M., Jensen, M., Linge, H., Lysa, A. & Larsen, E. 2006: Late Pleistocene glacial and lake history of northwestern Russia. *Boreas 35*, 394–424.

Lasabuda, A., Geissler, W. H., Laberg, J. S., Knutsen, S. M., Rydningen, T. A. & Berglar, K. 2018: Late Cenozoic Erosion Estimates for the Northern Barents Sea: Quantifying Glacial Sediment Input to the Arctic Ocean. *Geochemistry, Geophysics, Geosystems G3 19*, 4876–4903.

Lekens, W. A. H., Sejrup, H. P., Haflidason, H., Petersen, G. Ø., Hjelstuen, B. & Knorr, G. 2005: Laminated sediments preceding Heinrich event 1 in the Northern North Sea and Southern Norwegian Sea: Origin, processes and regional linkage. *Marine Geology 216*, 27–50.

Lucchi, R. G., Camerlenghi, A., Rebesco, M., Colmenero-Hidalgo, E., Sierro, F. J., Sagnotti, L., Urgeles, R., Melis, R., Morigi, C., Bárcena,

M. A., Giorgetti, G., Villa, G., Persico, D., Flores, J. A., Rigual-Hernández, A. S., Pedrosa, M. T., Macri, P. & Caburlotto, A. 2013: Postglacial sedimentary processes on the Storfjorden and Kveithola trough mouth fans: Significance of extreme glacimarine sedimentation. *Global and Planetary Change 111*, 309–326.

Lucchi, R. G., Sagnotti, L., Camerlenghi, A., Macrì, P., Rebesco, M., Pedrosa, M. & Giorgetti, G. 2015: Marine sedimentary record of Meltwater Pulse 1a along the NW Barents Sea continental margin. *The Journal of Arctic Geosciences 1*, 1–14.

Mangerud, J. & Landvik, J. Y. 2007: Younger Dryas cirque glaciers in western Spitsbergen: smaller than during the Little Ice Age. *Boreas 36*, 278–285.

Mangerud, J. & Svendsen, J. I. 1992: The last interglacial-glacial period on Spitsbergen, Svalbard. *Quaternary Science Reviews 11*, 633–664.

Mangerud, J., Bolstad, M., Elgersma, A., Helliksen, D., Landvik, J. Y., Lønne, I., Lycke, A. K., Salvigsen, O., Sandahl, T. & Svendsen, J. I. 1992: The last glacial maximum on Spitsbergen, Svalbard. *Quaternary Research 38*, 1–31.

Mangerud, J., Dokken, T., Hebbeln, D., Heggen, B., Ingólfsson, Ó., Landvik, J. Y., Mejdahl, V., Svendsen, J. I. & Vorren, T. O. 1998: Fluctuations of the Svalbard-Barents Sea Ice Sheet During the Last 150 000 Years. *Quaternary Science Reviews 17*, 11–42.

Mangerud, J., Kaufman, D., Hansen, J. & Inge Svendsen, J. 2008: Ice-free conditions in Novaya Zemlya 35 000–30 000 cal years B.P., as indicated by radiocarbon ages and amino acid racemization evidence from marine molluscs. *Polar Research 27*, 187–208.

Mitchum Jr, R. M., Vail, P. R. & Sangree, J. B. 1977: Seismic Stratigraphy and Global Changes of Sea Level, Part 6: Stratigraphic Interpretation of Seismic Reflection Patterns in Depositional Sequences. *In* Payton, C. E. (ed.): *Seismic Stratigraphy — Applications to Hydrocarbon Exploration 26*, 117–133, American Association of Petroleum Geologists, Tulsa.

Nielsen, T. & Rasmussen, T. L. 2018: Reconstruction of ice sheet retreat after the Last Glacial maximum in Storfjorden, southern Svalbard. *Marine Geology 402*, 228–243.

Ottesen, D. & Dowdeswell, J. A. 2009: An inter-ice-stream glaciated margin; submarine landforms and a geomorphic model based on marine-geophysical data from Svalbard. *Geological Society of America Bulletin 121*, 1647–1665.

Ottesen, D., Dowdeswell, J. A., Landvik, J. Y. & Mienert, J. 2007: Dynamics of the Late Weichselian ice sheet on Svalbard inferred from high-resolution sea-floor morphology. *Boreas 36*, 286–306.

Ottesen, D., Dowdeswell, J., Rise, L. & Ottesen, D. 2005: Submarine landforms and the reconstruction of fast-flowing ice streams within a large Quaternary ice sheet: The 2500-km-long Norwegian-Svalbard margin (57°-80°N). *Bulletin of the Geological Society of America 117*, 1033–1050.

Pope, E. L., Talling, P. J., Hunt, J. E., Dowdeswell, J. A., Allin, J. R., Cartigny, M. J. B., Long, D., Mozzato, A., Stanford, J. D., Tappin, D. R. & Watts, M. 2016: Long-term record of Barents Sea Ice Sheet advance to the shelf edge from a 140,000 year record. *Quaternary Science Reviews 150*, 55–66.

Prins, L. T., Andresen, K. J., Clausen, O. R. & Piotrowski, J. A. 2020: Formation and widening of a North Sea tunnel valley - The impact of slope processes on valley morphology. *Geomorphology 368*, 107347, https://doi.org/10.1016/j.geomorph.2020.107347.

Rasmussen, T. L. & Thomsen, E. 2013: Pink marine sediments reveal rapid ice melt and Arctic meltwater discharge during Dansgaard-Oeschger warmings. *Nature Communications 4*, 2849, https://doi.org/10.1038/ncomms3849.

Rasmussen, T. L., Thomsen, E., Ślubowska, M. A., Jessen, S., Solheim, A. & Koç, N. 2007: Paleoceanographic evolution of the SW Svalbard margin (76°N) since 20,000 ^{14}C yr BP. *Quaternary Research 67*, 100–114.

Rebesco, M., Wåhlin, A., Laberg, J. S., Schauer, U., Beszczynska-Möller, A., Lucchi, R. G., Noormets, R., Accettella, D., Zarayskaya, Y. & Diviacco, P. 2013: Quaternary contourite drifts of the Western Spitsbergen margin. *Deep-Sea Research Part I 79*, 156–168.

Rothwell, R. G. & Croudace, I. W. 2015: Twenty Years of XRF Core Scanning Marine Sediments: What Do Geochemical Proxies Tell Us? *In* Croudace, I. W. & Rothwell, R. G. (eds.): *Micro-XRF studies of*

sediment cores: Applications of a non-destructive tool for the environmental sciences, 25–102, Springer, Dordrecht.

Sarkar, S., Berndt, C., Chabert, A., Masson, D. G., Minshull, T. A. & Westbrook, G. K. 2011: Switching of a paleo-ice stream in northwest Svalbard. *Quaternary Science Reviews 30*, 1710–1725.

Sejrup, H. P., Hjelstuen, B. O., Torbjørn Dahlgren, K. I., Haflidason, H., Kuijpers, A., Nygård, A., Praeg, D., Stoker, M. S. & Vorren, T. O. 2005: Pleistocene glacial history of the NW European continental margin. *Marine and Petroleum Geology 22*, 1111–1129.

Sejrup, H. P., King, E. L., Aarseth, I., Haflidason, H. & Elverhøi, A. 1996: Quaternary erosion and depositional processes: Western Norwegian fjords, Norwegian Channel and North Sea Fan. *Geological Society Special Publication 117*, 187–202.

Skirbekk, K., Kristensen, D., Rasmussen, T., Koc, N., Forwick, M. & Skirbekk, K. 2010: Holocene climate variations at the entrance to a warm Arctic fjord: evidence from Kongsfjorden trough, Svalbard. *Geological Society, London, Special Publications 344*, 289–304.

Ślubowska, M. A., Koç, N., Rasmussen, T. L. & Klitgaard-Kristensen, D. 2005: Changes in the flow of Atlantic water into the Arctic Ocean since the last deglaciation: Evidence from the northern Svalbard continental margin, 80°N. *Paleoceanography 20*, PA4014, https://doi.org/10.1029/2005PA001141.

Ślubowska-Woldengen, M., Rasmussen, T. L., Koç, N., Klitgaard-Kristensen, D., Nilsen, F. & Solheim, A. 2007: Advection of Atlantic Water to the western and northern Svalbard shelf since 17,500 cal yr BP. *Quaternary Science Reviews 26*, 463–478.

Stuiver, M. & Reimer, P. J. 1993: Extended ^{14}C data base and revised CALIB 3.0 ^{14}C age calibration program. *Radiocarbon 35*, 215–230.

Svendsen, J., Alexanderson, H., Astakhov, V. I., Demidov, I., Dowdeswell, J., Funder, S., Gataullin, V., Henriksen, M., Hjort, C., Houmark-Nielsen, M., Hubberten, H., Ingolfsson, O., Jakobsson, M., Kjaer, K., Larsen, E., Lokrantz, H., Lunkka, J. P., Lysa, A., Mangerud, J., Matiouchkov, A., Murray, A., Moller, P., Niessen, F., Nikolskaya, O., Polyak, L., Saarnisto, M., Siegert, C., Siegert, M., Spielhagen, R. & Stein, R. 2004: Late Quaternary ice sheet history of northern Eurasia. *Quaternary Science Reviews 23*, 1229–1271.

Svendsen, J. I., Elverhøi, A. & Mangerud, J. 1996: The retreat of the Barents Sea Ice Sheet on the western Svalbard margin. *Boreas 25*, 244–256.

Sztybor, K. & Rasmussen, T. L. 2017: Diagenetic disturbances of marine sedimentary records from methane-influenced environments in the Fram Strait as indications of variation in seep intensity during the last 35 000 years. *Boreas 46*, 212–228.

Vorren, T. O. & Laberg, J. S. 1997: Trough mouth fans — palaeoclimate and ice-sheet monitors. *Quaternary Science Reviews 16*, 865–881.

Vorren, T. O., Laberg, J. S., Blaume, F., Dowdeswell, J. A., Kenyon, N. H., Mienert, J., Rumohr, J. & Werner, F. 1998: The Norwegian-Greenland Sea Continental Margins: Morphology and Late Quaternary Sedimentary Processes and Environment. *Quaternary Science Reviews 17*, 273–302.

Waelbroeck, C. and 62 others 2019: Age-depth model of sediment core MD95-2010 and associated dating uncertainty. *In* Waelbroeck, C. and 62 others (eds.) (2019): *Consistently dated Atlantic sediment cores.* PANGAEA, https://doi.org/10.1594/PANGAEA.900073.

Wessel, P. & Smith, W. 1998: New, improved version of generic mapping tools released. *Eos, Transactions American Geophysical Union 79*, 579.

Wohlfarth, B., Bjoerck, S., Funder, S., Houmark-Nielsen, M., Ingolfsson, O., Lunkka, J. P., Mangerud, J., Saarnisto, M. & Vorren, T. O. 2008: Quaternary of Norden. *Episodes 31*, 73–81.

Supporting Information

Additional Supporting Information to this article is available at http://www.boreas.dk.

Fig S1. Correlation of the magnetic susceptibility (MS) of GS10-164-09PC (red curve) with four selected cores from the Norwegian Sea (locations indicated by number and red circles on inset map, GS10-164-09PC marked by an orange circle) and the MS reference curve created by Jessen *et al.* (2010). The MS curve of GS10-164-09PC has been smoothed to ease the correlation. A total of eight new correlation points (identified in this study), in addition to four tie-points from Jessen *et al.* (2010) have been used for core correlation, where correlation-point 2–3 marks the stratigraphical position of the Last Glacial Maximum. The correlation points are peaks chosen owing to their characteristic signature and appearance in several cores (also outside of this study), and which could also be supported by the age control in this study (below). Core MD99-2304 (Labeyrie & Dokken 2005) is displayed in full, while MD95-2010 has been modified (cropped to include the upper 15 m, full extent 32.52 m, from Bassinot and Labeyrie 2003). Age estimates of correlation and tie-points are based on: (1) Jessen *et al.* (2010), (2) this study, and * the age control of the selected cores. *Age controls of the selected cores are based on: JM04-025PC (Jessen *et al.* 2010; Jessen & Rasmussen 2015, 2019), MD99-2304 (Ebbesen *et al.* 2007; Risebrobakken *et al.* 2014), MD95-2010 (Dokken & Jansen 1999; Dokken *et al.* 2014; Waelbroeck *et al.* 2019) and JM11-FI-19PC (Ezat *et al.* 2016; Hoff *et al.* 2016, 2019). The Heinrich events are based on Dokken & Hald (1996), Hemming (2004), Rasmussen *et al.* (2014), Ezat *et al.* (2016) and Hoff *et al.* (2019). Heinrich events H7a–H10 have been traced for the cores with an applicable stratigraphy, indicating that there is a regional MS signal, which can be traced at least within the Weichselian Glacial and probably further back in time.

Fig S2. Correlation of the δ^{18}O- and MS-curves of GS10-164-09PC and JM04-025PC. Correlation and tie-points on the MS curves follow those in Fig. S1. All radiocarbon dates are marked with black arrows and have been calibrated with Marine20. The ages given in red text are excluded from the age model. The interval covered by U9 (GDF) is marked with a purple border as it is considered instantaneous and not comparable between the two cores.

Data S1. The Age model of GS10-164-09PC. Description of how the age model is constructed.